



HAL
open science

Helium bubble nucleation and growth in alloy HT9 through the use of in situ TEM: Sequential He-implantation and heavy-ion irradiation versus dual-beam irradiation

Kai Duemmler, Ce Chris Zheng, Cedric Baumier, Aurélie Gentils, Djamel Kaoumi

► To cite this version:

Kai Duemmler, Ce Chris Zheng, Cedric Baumier, Aurélie Gentils, Djamel Kaoumi. Helium bubble nucleation and growth in alloy HT9 through the use of in situ TEM: Sequential He-implantation and heavy-ion irradiation versus dual-beam irradiation. *Journal of Nuclear Materials*, 2021, 545, pp.152641. 10.1016/j.jnucmat.2020.152641 . hal-03040741

HAL Id: hal-03040741

<https://hal.science/hal-03040741>

Submitted on 4 Dec 2020

HAL is a multi-disciplinary open access archive for the deposit and dissemination of scientific research documents, whether they are published or not. The documents may come from teaching and research institutions in France or abroad, or from public or private research centers.

L'archive ouverte pluridisciplinaire **HAL**, est destinée au dépôt et à la diffusion de documents scientifiques de niveau recherche, publiés ou non, émanant des établissements d'enseignement et de recherche français ou étrangers, des laboratoires publics ou privés.

Accepted in Journal of Nuclear Materials <https://doi.org/10.1016/j.jnucmat.2020.152641>

Helium Bubble Nucleation and Growth in Alloy HT9 through the use of *In Situ* TEM: Sequential He-Implantation and Heavy-Ion Irradiation versus Dual-Beam Irradiation

Kai Duemmler ^a, Ce Zheng ^a, Cedric Baumier ^b, Aurelie Gentils ^b, Djamel Kaoumi ^{a,*}

^a Department of Nuclear Engineering, North Carolina State University, Raleigh, 27607, NC, USA

^b Université Paris-Saclay, CNRS/IN2P3, IJCLab, Orsay, France

ABSTRACT

The formation of He bubbles in Ferritic/Martensitic steel HT9 is investigated through the use of *in situ* Transmission Electron Microscopy coupled with He implantation and heavy ion irradiation. Of particular interest is the effect of increasing He appm/dpa ratio on the formation and growth of the bubbles, as well as the effect of the sequential order of ion irradiation i.e. He-pre-implantation followed by heavy-ion irradiation versus true dual-beam irradiation. The role of He is discussed.

INTRODUCTION

HT9 is a Ferritic/Martensitic alloy envisioned as a candidate for structural and cladding applications in the next generation of nuclear reactors such as the sodium cooled fast reactor (SFR)[1-3]. One common reaction that occurs in nuclear reactors is the (n, α) decay whereby some elements can absorb a neutron and decay by producing an α particle (i.e. a He ion). There are 6 types of reactions that helium can undergo during irradiation: (1) helium can be trapped or thermally detrapped at a single, di or higher-order vacancy; (2) helium can be trapped at grain boundary or dislocation; (3) self-interstitial can replace a bonded helium to a single vacancy; (4) helium can form a vacancy-helium complex; (5) irradiation can displace trapped helium and (6) helium can migrate as an interstitial or in a di-vacancy [4]. An effect of the fourth kind of reaction protects vacancies from interstitials if 6 or more helium atoms can be combined with a vacancy cluster when this occurs, the interstitial atoms displacement field does not meet the energy requirement for the annihilation process thus stabilizing the vacancies [5]. It has been shown that helium-vacancy clusters migrate at about the same rate as the iron atoms at the surface of the clusters [6]. Another means that the helium-vacancy clusters are stabilized is that the emission of vacancies is suppressed but the emission of self-interstitial atoms is enhanced thus stabilizing the clusters [6]. A mean of migration for helium is in di-vacancies which can migrate at room temperature through substitutional mechanism [7]. These helium atoms are present due to helium implantation while the vacancies are present due to thermal equilibrium and/or produced by radiation. If trapped in the metal, He is known to stabilize cavities and lead to bubble formation and eventually contribute to swelling, although He is not absolutely necessary for cavities to form, in which case they are essentially voids caused by the accumulation of vacancies. The optimum stability of clusters occurs when there is an equal number of gas atoms to vacancies [7].

Because the helium is produced in the material at the same time as atomic displacements are produced by the energetic neutrons through point defect cascades, a rate of He appm/dpa can be calculated for a given material in a given position of the nuclear reactor. While the exact role of He on bubble/cavity formation/stabilization has been a topic of interest for while, it is not completely understood especially when the He appm/dpa ratio is added as a variable. To help elucidate this question we have conducted dual-beam in-situ ion irradiations of HT9 samples in-situ in a Transmission Electron Microscope (TEM) for different He appm/ratios at a given temperature (so not to add the temperature as a variable, which of course has an impact on swelling as well). In such experiments, the He is implanted while the heavy ions go through the TEM thin foils while generating the point defects.

Although, simultaneous dual-beam ion irradiation is the obvious approach to emulate reactor conditions where the formation of helium is concomitant with the formation of atomic displacements and point defects, there is also value to use “sequential” ion irradiation i.e. He ion implantation followed by heavy ion irradiation, or even the reverse order heavy ion irradiation followed by He implantation. Such experiments can indeed bring some light on the mechanisms at play in bubble/cavity formation and growth and particularly on the role of He as a nucleant or as a promoter of cavity growth. This brings up thereby the question if this order matters at all with the selected materials. Jublot-Leclerc et al. [8, 9] have suggested that it does matter in their study of stainless steel 316 L (SS 316 L). Thus, in this study, the effect of increasing He appm/dpa ratio on the formation and growth of the bubbles, as well as the effect of the sequential order of ion irradiation i.e. He-pre-implantation followed by heavy ion irradiation versus true dual-beam irradiation are investigated in HT9 *in situ* in the TEM.

EXPERIMENTS AND METHODS

2.1 Materials

The material used in this study is Ferritic/Martensitic steel HT9. The nominal chemical composition for this steel is given in table 1. Details about the heat used in this study and detailed characterization of the as received state can be found elsewhere [10-15]. It is basically composed of sub-micron laths with M23C6 carbides decorating prior-austenite grain boundaries and lath boundaries, as well as intragranular MX precipitates such as Vanadium rich nitrides.

Table 1: As received HT9 nominal and measured composition (wt.%) [13].

	Fe	Cr	Mo	Ni	Mn	W	V	Si	C	P	N	S	Cu	Al
Nominal	Bal.	11.8	1.03	0.51	0.5	0.5	0.33	0.21	0.21	0.008	0.01	0.003	-	-
Measured	Bal.	12.3	10.7	0.61	0.49	0.49	0.28	0.24	0.198	0.012	0.005	0.001	0.063	0.022

2.2 Sample Preparation and Irradiation experiments

The transmission electron microscopy (TEM) thin foils were prepared using focused ion beam (FIB) lift-out method at North Carolina State University. The samples were irradiated *in situ* with 4 MeV Au²⁺ ions and simultaneously implanted with 10 keV He⁺ ions at 430°C in the Tecnai G² 20 Twin microscope at the JANNuS-Orsay dual ion beam TEM facility [16]. The geometry of the set up at the JANNuS facility was such that the surface normal of the sample made a 22° angle with the helium beam and 23° angle with the ion beam as the two accelerators are 45° degrees apart.

Table 2 summarizes the ion irradiation conditions in terms of flux and fluences for both the gold ion and He ions along with the dose rate, helium implantation rate and the fluences reached. For the sequential experiment, the Helium was implanted *in situ* in the TEM followed by the gold ion irradiation. The three dual-beam experiments were done with different Helium appm/dpa ratios: 2.2, 22 and 100 He appm/dpa. For the sequential case, the final accumulated He concentration appm (331 appm) and the final dpa value (15 dpa) were chosen to give a ratio of 22 helium appm/dpa, equivalent to the dual beam case, to be able to compare for the same dpa level.

Table 2: Experimental Conditions:

	He Flux [ions/cm ² /s]	He implantation rate [appm/s]	dpa/s	Au Flux [ions/cm ² /s]	Final He fluence [ions/cm ²]	Final Au fluence [ions/cm ²]
Sequential implantation	3.00×10^{10}	3.54×10^{-2}	1.61×10^{-3}	4.05×10^{11}	2.80×10^{14} Before Au irradiation	3.77×10^{15} (15 dpa)
2.2 He appm/dpa	3.00×10^9	3.54×10^{-3}	1.61×10^{-3}	4.05×10^{11}	2.80×10^{14} (at 15 dpa)	3.77×10^{15} (15 dpa)
22 He appm/dpa	3.00×10^{10}	3.54×10^{-2}	1.61×10^{-3}	4.05×10^{11}	2.80×10^{14} (at 15 dpa)	3.77×10^{15} (15 dpa)
100 He appm/dpa	1.40×10^{11}	1.65×10^{-1}	1.65×10^{-3}	4.15×10^{11}	1.27×10^{15} (at 15 dpa)	3.77×10^{15} (15 dpa)

The displacement rates produced by the implantation of helium ions and the irradiation by gold ions were calculated using SRIM [17] in “quick calculation” mode using displacement threshold energies of 40 eV and 28 eV for Fe and Cr respectively. The displacements caused by the helium ions were two to three orders of magnitude smaller than the displacements caused by the gold ions thus were deemed negligible, as can be seen in figure 1.B. The implantation depth of both the gold and helium ions can also be seen below in figure 1. It can be noted that all the helium is implanted in the first 100 nm, which is the thickness of the sample while there is little to no gold ions implanted in this thickness as seen in figure 1.A.

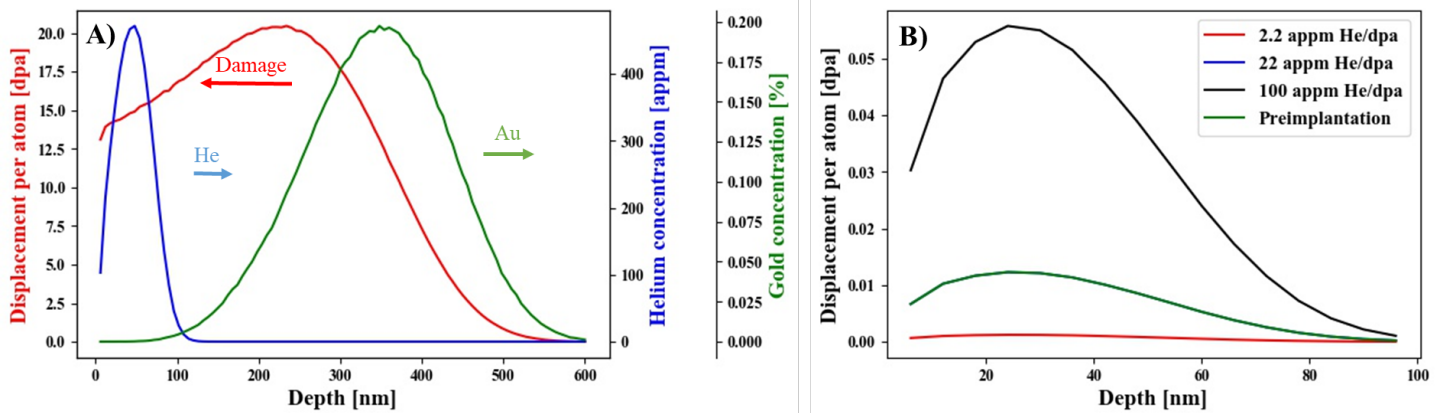


Figure 1: SRIM calculation for implantation depth into the HT9 samples by the 10 keV He⁺ and 4 MeV Au²⁺ ions. A) shows the damage profile of the gold ions, the percentage gold and the

helium concentration for the entire range of gold and the sample thickness while B) shows the damage induced by implantation of helium.

2.3 Methods for Bubble Measurements

2.3.1 Imaging/detection of the bubbles

It is well known that when bubbles are too small (less than 5 nm) they are difficult to image in focused bright-field imaging mode whether in dynamical or kinematical conditions [18]. In order to make them visible if they are in fact present in the sample is to image in either under- or over-focused conditions as the bubbles will appear in the out-of-focus conditions due to phase-contrast and weak absorption. This phase shift is also the cause of Fresnel fringes which help render the bubble visible [18]. In the over-focused image a white fringe appears around a dark center and in the under-focused condition a black fringe appears around a white center [18]. Thus, by going through focus one can thus establish the presence of bubbles even when they are too small to be imaged in focused conditions. Thus for each dose point of interest a series of under focused, at focus, and over focused images were taken.

2.3.2 Bubble density and size measurements

To count and measure the bubbles on the images the software ImageJ was used. The measurements were done consistently on the under-focused images. If there was uncertainty about the “legitimateness” of a bubble (due to imaging conditions and possible radiation damage interference), it was noted on the measurement sheet so that when plotting the bubble density, the error bar was determined by using the number of “certain” bubbles as the lower end and the total number of bubbles counted as the upper end of the error bar. Of course, the densities were calculated by dividing the number of bubbles in the measured area by the corresponding volume (area x thickness of the sample which was ~100 nm).

As for the bubble size, it was measured with ImageJ under which the bubbles were assumed to have an elliptical or oval shape. The inner white area was measured by the tool and the diameter of the disc of equivalent area was calculated and taken as the equivalent bubble diameter. An error of ~10 percent is assumed on the measured size when using the method described above, with measurements done on the under focused images [18]. Note that in order to be able to compare size measurements between dose points and experiments in which the defocusing amount was not the same, a correction was applied using the parameter $\beta = \frac{\Delta f}{\pi k_0 r_0^2}$ [18] where Δf is the defocus value, k_0 is the electron wavevector [λ^{-1}] and r_0 is the measured bubble radius.

EXPERIMENTAL RESULTS

Overall, during the experiments, the dpa ranged from 0 to 31 while the accumulated amount of He was between 33 and 2600 appm He with all the experiments carried out at 430°C. Figures 2 and 3 give examples of the images that were analyzed counted for the sequential irradiation (i.e. He implantation followed by Au irradiation) and for the dual-beam irradiation case at 22 He appm/dpa; similar approach was done for the other cases. The bubble density and measurements for each experiment are shown in Table 3. Within the table “NO” is written where

no bubbles were observed. It can be seen that a threshold of helium concentration for bubble formation is reached between 221 appm and 331 appm helium. There is also a threshold of He concentration and associated dpa level for the dual beam case at 2.2 He appm/dpa for bubble formation whereas bubbles are present at all dose levels for the higher He appm/dpa ratios, as can be seen in figure 3 which shows the 22 helium appm/dpa case. Figure 4 shows the size distributions for the 4 experiments as a function of dose and accumulated He appm. The distributions are all monomodal.

In figure 5, the bubble size distributions for the dual beam case (at 22 He appm/dpa) at 15 dpa and 330 accumulated He appm is compared with the bubble size distribution for the sequential irradiation case at 15 dpa after implantation of 331 appm He since both have the same effective 22 He appm/dpa. Table 4 reports the average measured bubble size and number density for both cases. It can be seen that the dual-beam experiment produces bubbles with larger sizes than the pre-implantation of helium followed by the gold ion irradiation but less bubbles.

Table 3. Bubble Average bubble size and number density for all experiments

Dual / Sequential irradiation (He appm/dpa)	Dose in dpa and cumulated He concentration in appm	Total # bubbles counted	Average size [nm]	density [10^{23} m^{-3}]
Sequential irradiation i.e. He implantation then Au ion irradiation 430°C	0 dpa 221 appm He	NO	NO	NO
	0 dpa 331 appm He	115	1.8±0.2	0.34±0.05
	10 dpa 331 appm He	222	1.9±0.2	0.69±0.07
	15 dpa 331 appm He	350	1.8±0.2	1.15±0.08
Dual ion beam 430°C (2.2 He appm/dpa)	15 dpa 33 appm He	NO	NO	NO
	20 dpa 44 appm He	NO	NO	NO
	26 dpa 57.2 appm He	NO	NO	NO
	31 dpa 68.2 appm He	302	2.1±0.2	1.88±0.2
Dual ion beam 430°C (22 He appm/dpa)	15 dpa 330 appm He	177	2.4±0.2	0.6±0.03
	20 dpa 440 appm He	220	2.1±0.2	0.74±0.03
	26 dpa 572 appm He	253	2±0.2	0.8±0.09
Dual ion beam 430°C (100 He appm/dpa)	10 dpa 1000 appm He	230	1.7±0.2	1.75±0.29
	20 dpa 2000 appm He	400	1.3±0.1	2.98±0.58
	26 dpa 2600 appm He	528	1.5±0.1	4.43±0.26

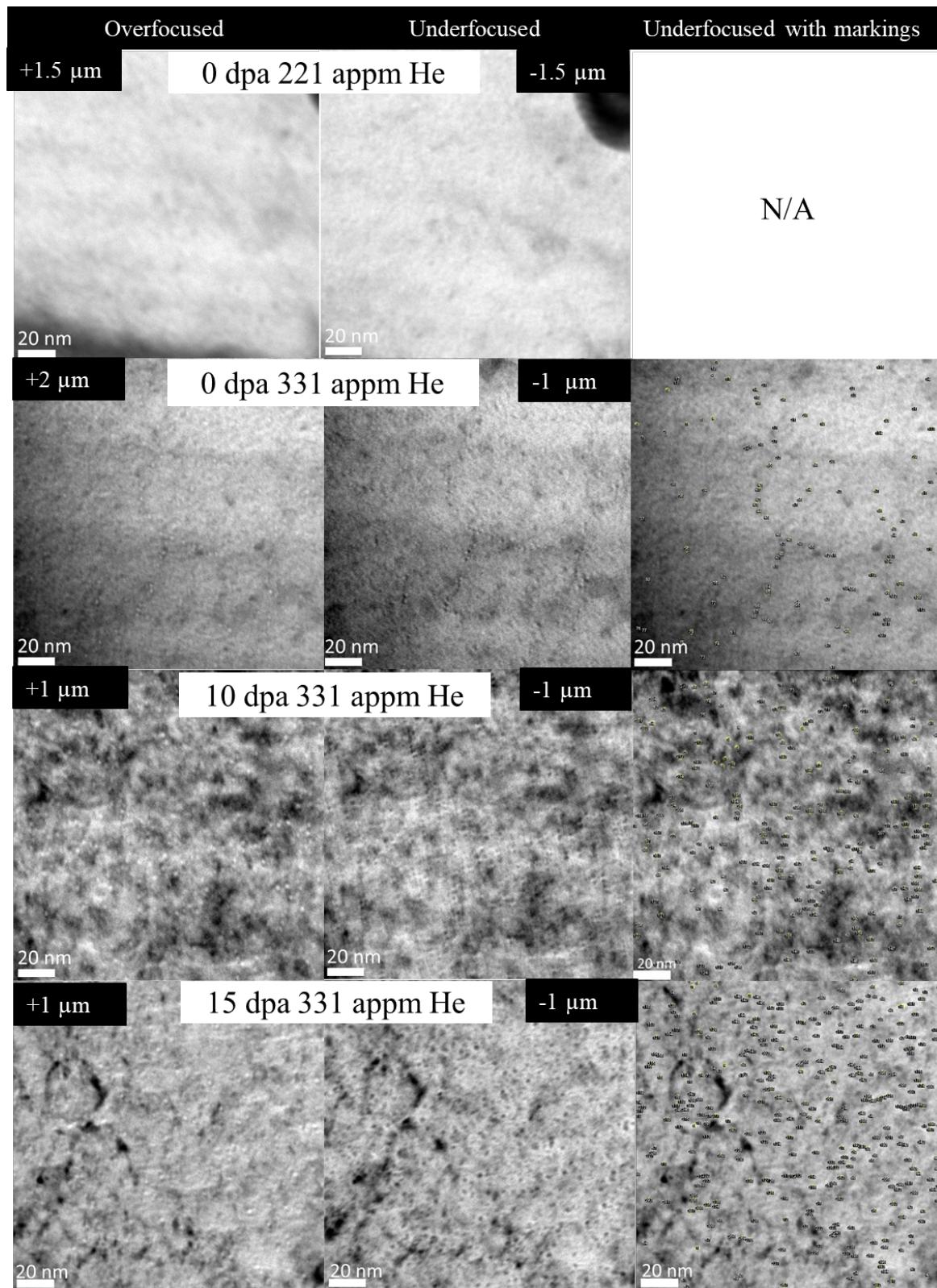


Figure 2: TEM underfocused and overfocused imaging evidencing bubbles for the case of sequential implantation of 10 keV helium ions followed by 4 MeV gold ions. Note that the final cumulated He appm and dose correspond to 22 appm/dpa.

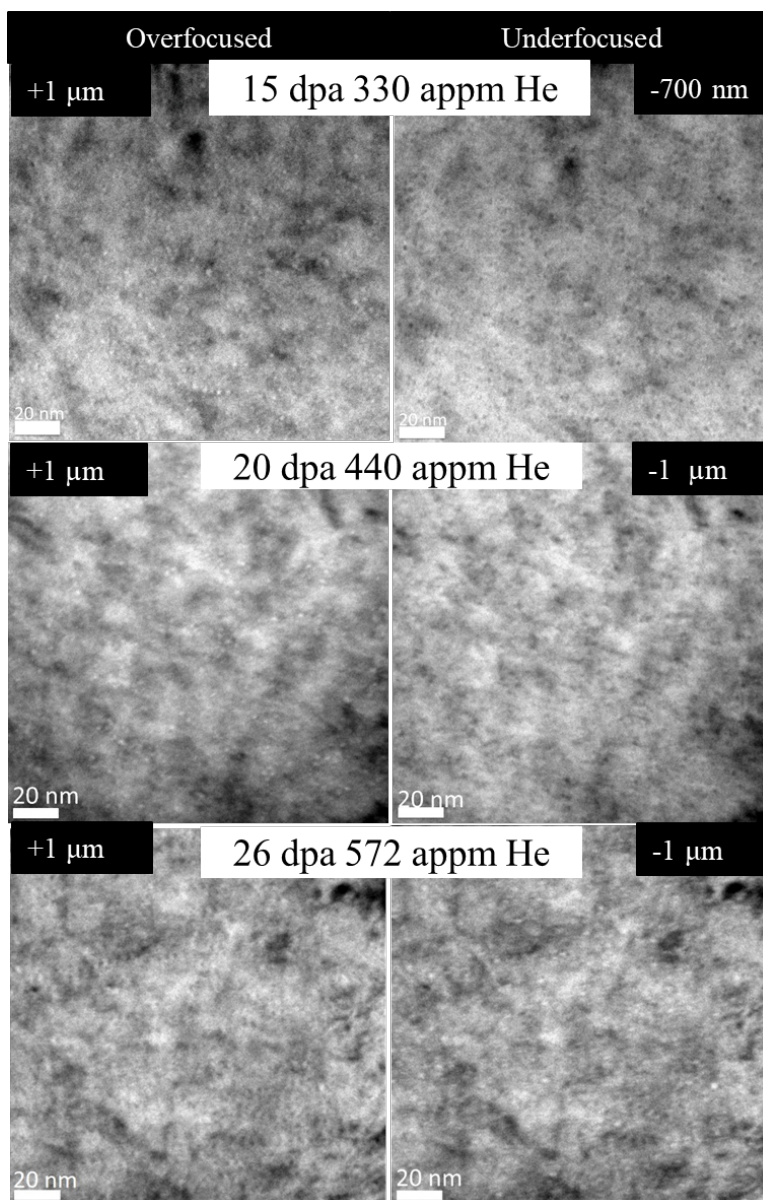


Figure 3: TEM underfocussed and overfocussed imaging for the counting of the bubbles in the case of dual-beam implantation of helium and gold ions for 15 to 261 dpa and 330 to 572 appm He with a helium appm/dpa ratio of 22.

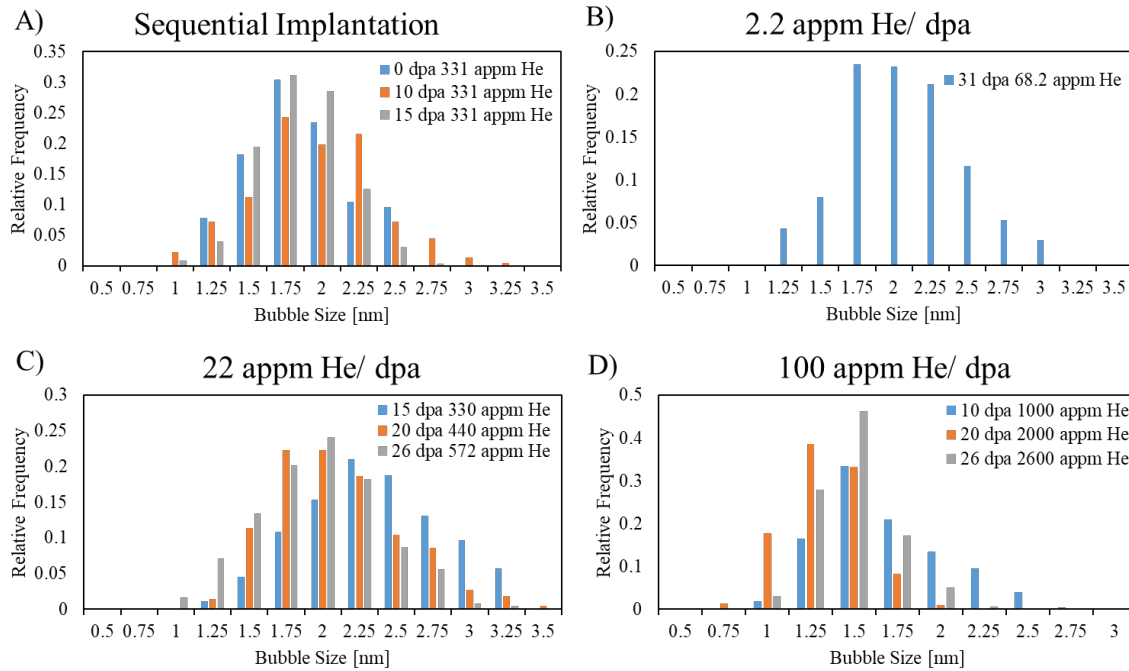


Figure 4: Bubble size distribution for each experiment as a function of dose.

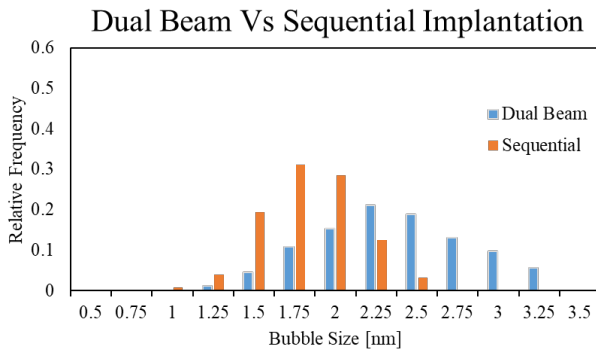


Figure 5: Comparing the bubble size distributions of the dual-ion beam case and the sequential ion irradiation case.

Table 4: Dual-beam vs sequential ion irradiation, showing the density and average bubble size for dual-beam 15 dpa and 330 appm He and the sequential for 15 dpa and 331 appm He.

Dual-Beam vs Sequential	Bubble Size [nm]	Bubble Density [# x10 ²³ /m ³]
Dual-Beam	2.4±0.2	0.6±0.03
Sequential	1.8±0.2	1.2±0.08

The effect of increasing helium appm/dpa ratio on the nucleation and growth of the He bubbles was also studied during the dual-beam experiments as reported Figure 6, the overall trend is that the bubble size decreases as the Helium appm/dpa ratio increases for a given dose and

conversely the density of bubbles increases with increasing He appm/dpa. Figure 6 also shows the resulting swelling percentage. Note that to calculate the density the volume was considered to be simply the area of the TEM picture over which the measurements were done times the thickness of the sample (~ 100 nm), and this does not take into account the depleted zones that are expected to form near the free surfaces as discussed in section 4.3, therefore the values of bubble densities and swelling percentage plotted here are expected to be underestimated but this should not affect the trends that are commented.

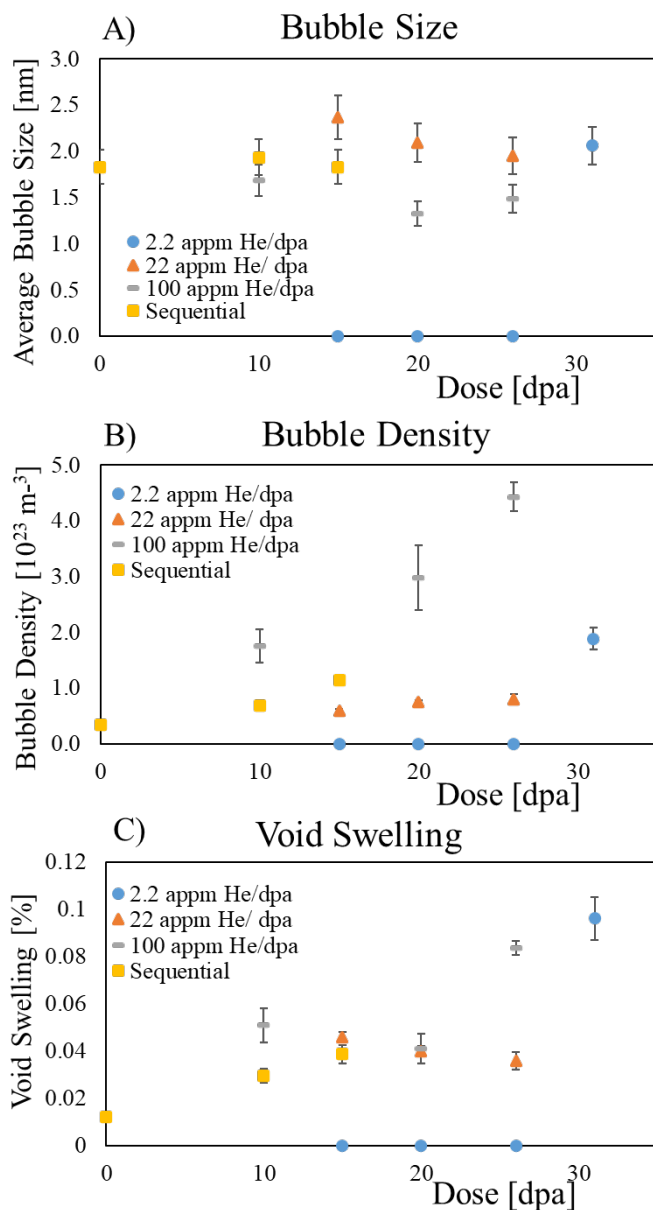


Figure 6: Average bubble size (A), bubble density (B) and swelling fraction ($\Delta V/V$) as a function of the dose (dpa) for each studied conditions (simultaneous helium and gold ion beams for three indicated flux, and sequential helium ion implantation followed by gold ion irradiation).

DISCUSSION

4.1 Effect of sequential irradiation vs. dual-beam irradiation on bubble size and density

The results show that during sequential irradiation where HT9 is implanted with 331 appm helium, followed by gold ion irradiation to 15 dpa, the He bubbles are smaller but more numerous than in the “equivalent” case of the dual-beam (15 dpa with 330 appm helium). The nucleation rate is higher for the sequential helium implantation than for the dual-beam but the bubbles grow more under dual-beam. Also, as seen in the bubble size distribution shown in figure 5, sequential irradiation has a smaller spread of sizes compared to the dual-beam. The same trend was observed in a study conducted by Packan and Farrell [19] at 900 K (627°C) in Alloy P7 (Fe-17Cr-16.7Ni-2.5Mo) (a similar austenitic steel to 316 SS) where the cavity diameter increased in the order of (i) pre-implantation at room temperature (RT), (ii) pre-implantation at 900K, (iii) single beam irradiation, (iv) dual-beam irradiation, and finally (iii) triple beam irradiation. The beams used were 4.0 MeV Ni ions, helium at a rate of 20 He appm/dpa and deuterium at a rate of 50 D appm/dpa to doses of 1, 10 and 70 dpa. As for the bubble density in [19], both pre-implanted cases resulted in higher number density of bubbles than the single beam, dual beam and triple beam cases. Both these trends held for 1 to 70 dpa in their study. The “nucleant” role of helium in dual-beam irradiation seems less efficient than in sequential irradiation as the concomitant point defect formation may enhance the mobility of the implanted He helping it migrate more easily to existing bubbles; as a result, during dual-beam irradiation bubbles are larger as implanted helium ions are continuously absorbed by pre-existing bubbles instead of creating new nucleation sites [19].

There have also been experiments done on 304 SS comparing dual-beam and pre-implanted cases of 200 appm helium, with three study cases (i) pre-implantation at 25 °C, (ii) pre-implantation at temperature (650, 700 and 750 °C), and (iii) dual-beam irradiation (at 80 He appm/dpa) with 28 MeV Si⁶⁺ to a dose of ~40 dpa [21, 22]. They observed that dual-beam irradiation led to an average bubble size smaller than for the pre-implantation at temperature but larger than for the case of pre-implantation at room temperature, indicating an effect of the pre-implantation temperature [21]. The number densities had the opposite trends. The trend when comparing dual beam and pre-implantation at temperature is in contrast with in our study and with the previously mentioned study [19]. However, this difference may come from the concomitant phase transformations happening in 304; in fact in [19], unidentified “acicular precipitates” were reported to form along with the cavities have coupled growth [23]. However the effect of pre-implantation temperature was not investigated in our study, but one would indeed expect to have a larger bubble density with smaller sizes in the room temperature pre-implanted case since, although implanted helium can migrate in vacancy complexes at room temperature through substitutional mechanism [7], its mobility is expected to be less than at higher temperatures and thus more embryos may form with accumulated He [19]. In the end it is the local helium mobility during implantation and the localized vacancy flux to the embryos during ion bombardment that determine whether or not a cavity will grow to a visible (TEM) size for the pre-implantation cases.

Thus, regardless of the crystal structure (austenitic (304SS, and P7) or F/M), there is a difference between sequential irradiation and dual beam irradiation in terms of the resulting He bubble size and number density for equivalent He implantation and dpa level. This difference between pre-implantation versus dual implantation can be due to the continuous absorption of helium by pre-existing cavities in dual-beam irradiation or it could result from the supersaturation of vacancies before irradiation damage [19, 24]. In our case, since the level of vacancy concentration due to the He implantation is rather negligible (especially compared with the vacancies induced by the heavy ions), it is more likely that the difference arises from the former hypothesis that helium is continuously absorbed by pre-existing bubbles during the dual-beam irradiations. The temperature effect suggested by [21] needs further investigation.

4.2 Effect of sequential irradiation order and the role of Helium

Our sequential irradiation experiment consisted of He implantation followed by heavy ion irradiation; when compared to dual-beam irradiation, it gave similar trends (as described above) with similar experiments in the literature done in the bulk or on other materials (including austenitic alloys). Indeed, in the study on alloy P7 already mentioned earlier it was shown that dual-beam irradiation produced larger bubbles than pre-implantation of both at RT or irradiation temperature followed by irradiation but had a lower number density [19]. In the study by Farrell and Packan [24] on the same alloy when they were testing the effect of temperature it was shown that single ion-beam (no helium) had a smaller density of cavities compared to dual-beam and triple-beam (helium + hydrogen + nickel ion) irradiation for all temperatures at 1 and 70 dpa when it had cavities. At 1 dpa, the observed trend was that single nickel irradiation resulted in larger cavities than for the dual-beam but the size decreased at 1025 K and became smaller than the dual-beam case as there were no visible cavities.

It is worth comparing these trends to a recent study where heavy ion irradiation was done before the implantation and where the authors compared their results with dual-beam irradiation. Indeed, in a study on 316L [8, 9], Jublot-Leclerc et al. compared (i) dual-beam irradiation using 4 MeV Au^{2+} and 10 keV He^+ ions, (ii) single ion irradiation (without He), and heavy ion irradiation followed by helium implantation at 450°C and 550°C. They reported that the dual-beam (250 appm/dpa) and single irradiation (only Au^{2+} irradiation) led to cavities with similar sizes at 450°C. In their case study with post helium implantation at 550 °C, the helium does not cause more nucleation but grows the existing cavities and helps with the coalescence of cavities. The cavities grow by the direct absorption of helium atoms injected into the matrix [8]. This shows that the sequential order of irradiation matters, and it leads us to discuss the role of helium and the role of heavy ion irradiation in such experiments.

In the literature, sequential ion irradiation (i.e. implantation then irradiation) was also done on T91 with various levels of implanted He (0, 1, 10, 100, or 1000 appm) into the sample using 400 keV He ions at room temperature. Then the samples were irradiated to dpa levels ranging from 45 to 356 dpa at 460°C [25]. They observed that as the helium concentration increased for the same dose level, the bubble size would decrease while the density would increase. The role of helium in the sequential irradiation i.e. implantation then irradiation is to act as a nucleant. When helium is inserted during dual-beam irradiation it can both nucleate new cavities and be absorbed by the pre-existing ones to promote growth. In the case found in the literature where irradiation was followed by implantation, helium was only absorbed by the existing cavities but did not nucleate any new cavities.

As for the role of Heavy ion irradiation after helium implantation, during our experiment after the HT9 sample was implanted with 10 keV helium ions to a concentration of 331 appm He, bubbles were already present before the sample was irradiated with the Au ions. Interestingly the average bubble size did not change after the heavy ion irradiation as can be seen in figure 6A, however when looking at the size distribution (shown in figure 4), it became broader and slightly shifted to the right. Also, there was a clear increase in the density of bubbles as seen in figure 6B. There are two methods for the density to increase. The first would be to split the existing bubbles with the irradiation damage. Even if such a mechanism was possible, this would be rather unlikely since the size distribution shifted to the right not left. If the larger bubbles were being split, even larger bubbles would not form, which was in fact observed. The other scenario would be that the point defects (essentially the vacancies produced by the ion irradiation) enhance the mobility of the helium that was trapped in solution or in clusters (that were not TEM visible prior to the heavy ion irradiation). This would allow for the creation of new bubbles and to grow the existing ones and it could also explain the broadening of the size distribution.

4.3 Effect of helium appm/dpa rate on the He bubble size and number density during dual-beam irradiations:

The influence of having different He implantation rates on the nucleation and growth of the He bubbles was also studied during the dual-beam experiments. Based on Figure 6, the overall trend observed is that the bubble size decreases as the helium appm/dpa ratio increases for a given dose and conversely the density of bubbles increases with increasing He appm/dpa. This trend observed in our study is also reported in the literature on different materials (i.e. F/M steels as well as austenitic steels). For instance, Monterrosa et al. who carried out dual beam irradiations on bulk HT9 at 460 °C with 5 MeV Fe²⁺ ions with helium appm/dpa from 0 to 0.2 with dpa values up to 188 dpa, followed by *ex situ* characterization [26] also reported a bubble size decrease and a density increase as the He appm/dpa ratio increased in the specific ranges of appm/dpa ratio values investigated. This shows by the way that *in situ* TEM ion irradiations led to similar trends as bulk ion irradiations in the same material. It is worth emphasizing that it is not the absolute values of bubble densities or the swelling strain values that are compared with the bulk irradiations in the Monterrosa study, but the trends and the effect of He implantation rate and sequence on those trends. Of course, when comparing bulk and in-situ (thin films) experiments one should always consider the effect of free surfaces which are powerful sinks and play a bigger role in thin-foil experiments since any helium atom within a certain range of a free surface will escape to this surface creating a depleted zone[20], which may change the thickness of the area of interest by a significant margin, for instance in Jublot-Leclerc such depleted zone was ~20 nm [8]. This being said, in our case, our experiments were done at the same temperature with samples of about the same thickness, so it is reasonable to assume that such depleted zone would be of similar thickness for each sample so that the trends registered within our experiments are reliable from that prospect.

The same trend was reported in other alloys including austenitic alloys such 316 SS [27, 28]. In [28] Katoh et al. compared different He appm/dpa rates up to 25 dpa at a temperature of 873 K, using 4 MeV Ni³⁺ and 1 MeV He²⁺ ions in AISI 316 bulk samples. They also reported that the higher the appm/dpa rates the larger the bubble density. In addition, for the same helium appm/dpa, an increasing dose would increase the bubble density, which is also observed in our

study. There is also a linear relationship between the bubble densities at a given dose as a function of He appm/dpa. This is also an observed trend in this study.

In another austenitic alloy (Fe-16.22Ni-14.57Cr-2.37Mo-1.79Mn) [29], which is basically a titanium modified stainless steel 316 alloy, Sekimura et al. studied the effects of two different dual-beam implantation rates (15 and 75 He appm/dpa) and compared it to pre-implantation of 20 appm He and irradiation by a 0.4 MeV Al⁺ ions to 50 dpa. They observed that the larger the He appm/dpa ratio, the larger the density over the temperature range investigated from 427 to 650 °C. The bubble size in their study was however similar for both dual-beam conditions along with the pre-implanted and single beam irradiation [29], maybe due to the presence of Ti(C,N) precipitates. In addition, they observed an influence of the irradiation temperature on the bubble size, with similar bubble sizes in their lower range of temperatures for both He appm/dpa ratios whereas at elevated temperatures the 75 appm He/dpa yielded larger bubbles than 15 appm He/dpa. This effect of temperature may need further investigation since our study was only done at one fixed temperature. This being said, one ought to be careful when comparing results between different materials when the microstructure can be drastically different; for instance Ti-modified 316 SS (such as studied in [29]) is known to have a large density of small Ti(C,N) precipitates which can definitely alter the nucleation rate of He bubbles and affect their kinetics of growth since they can act as recombination centers for point defects.

The overarching trend for bubble density is that as the He appm/dpa increases so does the density of the bubbles. Moreover, the larger the He appm/dpa the more responsive the bubble density becomes to dpa. Based on our observations, two observations can be made: (i) as the dose and helium concentration increases the density of cavities increases; and (ii) as the He appm/dpa increases the bubble size gets smaller; indeed, at the low He appm/dpa ratio, bubbles did not become visible until doses greater than 26 dpa with 57.2 appm He whereas for the larger appm/dpa ratio, there is sufficient helium to stabilize the vacancies and grow into visible bubbles at a lower dose. These two trends are supported by other studies of dual-beam experiments [26, 27, 30].

4.4. On the bubble size distribution shape (unimodal versus bimodal):

In this study done *in situ* in the TEM at 430°C, all bubble size distributions were monomodal with sizes less than 5 nm, which suggests that the bubbles were not able to reach the critical radius or the critical number of helium atoms within the bubble to allow for larger bubbles to grow to form the bimodal distribution. Based on the literature, for a given He appm/dpa ratio the formation of a bimodal distribution depends on the temperature [31, 32], which was also observed in the BOR60 irradiations of the same HT9 alloy [12] and possibly on dose [13]. The dose rate may also affect the size distribution shape but there is lack of studies on the matter. In our studies [10,12,13], the bimodal void size distribution was observed in HT9 at 690K (~ 417 °C) at ~18 dpa under neutron irradiation [12] but irradiating the same alloy with dual ion beam in bulk at a similar temperature and dose (432 °C to 16.6 dpa) resulted in a unimodal distribution [10] and in the current study, irradiating the same alloy with dual beam in a thin foil at the same temperature and similar dose (430 °C and 15 dpa) also gives a unimodal distribution; from that perspective the current study (in the thin foil geometry) shows the same effect of higher dose rate of the size distribution shape i.e. an apparent “suppression” or delaying of the occurrence of the bimodal size distribution aspect. A quantitative understanding of how the dose rate affects the microstructural evolution of cavities is still lacking in the literature as pointed out in [20].

As far as the effect of the He appm/dpa on the bubble size distribution shape, the discussion can be geared towards the bubble-to-void conversion model. In austenitic alloys, Katoh et al. [30] reported that the He appm/dpa ratio does have an effect on the bubble-to-void conversion. In such a model, a bubble is a cavity which has not reached the critical radius to shift to bias growth; once it reaches that radius it is called a void. In low He appm/dpa ratios (4-15 He appm/dpa), the transition is expected to occur faster than for higher ratios (50 He appm/dpa). This was supported by the results by Manterrosa et al. in F/M steels [26] [40]. What changes in the microstructure is the required critical radius for the bias growth model to play a role. In the case of higher helium appm/dpa, the vacancy clusters' growth is hindered due to reduced net vacancy flux [30]. It was suggested by Stoller [33] that high cavity sink strength causes an increase in the recombination of point defects at the cavity, which in turn reduces the saturation of point defects and hinders bubble-to-void conversion by increasing the critical number of gas atoms for void formation. This can be exacerbated by a second method of delaying the bubble-to-void conversion which is by diluting the helium and vacancies to a large number of cavities to lower the rate at which bubbles reach the critical size. A method to cause this is fine precipitates as bubbles will form there [34]. When helium is co-implanted with ion irradiation damage the interstitial atoms created by ion damage compete with helium to interact with the vacancies [4]. If the interstitials are faster the vacancies are annihilated or else the helium can interact and be trapped with a vacancy or high order vacancies and form helium-vacancy complexes[4]. With higher He appm/dpa ratio the latter may happen, explaining why the transition would happen more slowly.

CONCLUSIONS

In this study, the formation of He bubbles in HT9 alloy was investigated through the use of *in situ* Transmission Electron Microscopy coupled with He ion implantation and heavy ion irradiation. In such experiments, helium is implanted to emulate the (n, α) reactions that occur in a nuclear reactor.

To investigate the effect of increasing the He appm/dpa ratio on the formation and growth of the bubbles, three different helium appm/dpa rates were probed during the *in situ* dual ion beam irradiations: 2.2, 22 and 100, respectively. It was observed that the larger the rate of helium/dpa the larger the bubble density and the smaller the size of the bubbles. The bubble density showed a linear increase with dose (dpa) and He concentration (appm) for the ranges investigated. Also it is worth mentioning that the "threshold" dose (dpa) at which visible bubbles can be imaged with TEM decreases with increasing He appm/dpa ratio.

During a sequential ion irradiation where helium implantation was followed by heavy ion irradiation, the role of helium as a "nucleant" was evident where visible bubbles were imaged at 331 He appm before the heavy ion irradiation started although the vacancy concentration was very low (i.e. low dpa due to He alone); the subsequent heavy ion irradiation did not increase the size of bubbles, however, it increased their density. This is to be put in contrast with the dual-beam case where visible bubbles were imaged at lower accumulated He appm concentration with the help of the vacancies produced by the concomitant heavy ion irradiation. In the case where the same dose and cumulated He concentration was achieved through dual beam irradiation (at 22 He appm/dpa) and through sequential irradiation (i.e. 15 dpa and 330 appm He), the dual-beam irradiation seems to lead to a smaller density of bubbles but of larger sizes for a given dose

(in dpa). The ability of helium to nucleate new bubbles depends on the initial presence of voids/cavities: its role as a nucleant is less effective when cavities are already present, in which case He is more likely to feed the existing cavities rather than to nucleate new ones. Overall the role helium in bubble formation and growth of bubbles and its dependence of the sequential order of the irradiation as well as temperature (an effect not investigated in this study) could use further investigation. Particularly such in-situ TEM experiments could be used to investigate the possible role of dislocation lines and irradiation induced dislocation loops on the nucleation process.

ACKNOWLEDGEMENTS

This work was supported as part of FUTURE (Fundamental Understanding of Transport Under Reactor Extremes), an Energy Frontier Research Center funded by the U.S. Department of Energy, Office of Science, Basic Energy Sciences. FIB sample preparation and post-irradiation STEM characterizations were performed at the Analytical Instrumentation Facility (AIF) at the North Carolina State University. The AIF is a member of the North Carolina Research Triangle Nanotechnology Network which is supported by the State of North Carolina and the National Science Foundation (award number ECCS-1542015). The JANNuS-Orsay technical staff is acknowledged for their help during the *in situ* ion implantations/irradiations. This experiment was partly supported by the French Accelerator Network EMIR for Materials and Irradiation studies through project number 17-2051.

REFERENCES

1. Garner, F.A., M.B. Toloczko, and B.H. Sencer, *Comparison of swelling and irradiation creep behavior of fcc-austenitic and bcc-ferritic/martensitic alloys at high neutron exposure*. Journal of Nuclear Materials, 2000. **276**(1): p. 123-142.
2. Klueh, R.L. and A.T. Nelson, *Ferritic/martensitic steels for next-generation reactors*. Journal of Nuclear Materials, 2007. **371**(1): p. 37-52.
3. Zinkle, S.J. and G.S. Was, *Materials challenges in nuclear energy*. Acta Materialia, 2013. **61**(3): p. 735-758.
4. Ghoniem, N., et al., *Theory of helium transport and clustering in materials under irradiation*. Journal of Nuclear Materials, 1983. **117**: p. 96-105.
5. Beeler, J.R., *Radiation Effects Computer Experiments*. 2012: Elsevier Science.
6. Morishita, K., R. Sugano, and B.D. Wirth, *MD and KMC modeling of the growth and shrinkage mechanisms of helium-vacancy clusters in Fe*. Journal of Nuclear Materials, 2003. **323**(2): p. 243-250.
7. Reed, D., *A review of recent theoretical developments in the understanding of the migration of helium in metals and its interaction with lattice defects*. Radiation Effects, 1977. **31**(3): p. 129-147.
8. Jublot-Leclerc, S., et al., *Cavity nucleation and growth in dual beam irradiated 316L industrial austenitic stainless steel*. Journal of Nuclear Materials, 2017. **494**: p. 240-251.
9. Jublot-Leclerc, S., et al., *TEM study of the nucleation of bubbles induced by He implantation in 316L industrial austenitic stainless steel*. Journal of Nuclear Materials, 2015. **466**: p. 646-652.
10. Zheng, C. and D. Kaoumi, *Radiation-induced swelling and radiation-induced segregation & precipitation in dual beam irradiated Ferritic/Martensitic HT9 steel*. Materials Characterization, 2017. **134**: p. 152-162.

11. Zheng, C., et al., *Radiation induced segregation and precipitation behavior in self-ion irradiated Ferritic/Martensitic HT9 steel*. Journal of Nuclear Materials, 2017. **491**: p. 162-176.
12. Zheng, C., et al., *Microstructure response of ferritic/martensitic steel HT9 after neutron irradiation: Effect of temperature*. Journal of Nuclear Materials, 2020. **528**: p. 151845.
13. Zheng, C., et al., *Microstructure response of ferritic/martensitic steel HT9 after neutron irradiation: effect of dose*. Journal of Nuclear Materials, 2019. **523**: p. 421-433.
14. Zheng, C., S. Maloy, and D. Kaoumi, *Effect of dose on irradiation-induced loop density and Burgers vector in ion-irradiated ferritic/martensitic steel HT9*. Philosophical Magazine, 2018. **98**(26): p. 2440-2456.
15. Zheng, C., et al., *Correlation of in-situ transmission electron microscopy and microchemistry analysis of radiation-induced precipitation and segregation in ion irradiated advanced ferritic/martensitic steels*. Scripta Materialia, 2019. **162**: p. 460-464.
16. JANNuS (Joint Accelerators for Nano-science and Nuclear Simulation)
[Http://jannus.in2p3.fr](http://jannus.in2p3.fr) and [Http://www.csns.in2p3.fr/MET](http://www.csns.in2p3.fr/MET).
17. Ziegler, J.F., M.D. Ziegler, and J.P. Biersack, *SRIM – The stopping and range of ions in matter (2010)*. Nuclear Instruments and Methods in Physics Research Section B: Beam Interactions with Materials and Atoms, 2010. **268**(11): p. 1818-1823.
18. M L Jenkins, M.A.K., *Characterization of Radiation Damage by Transmission Electron Microscopy*, in *Characterization of Radiation Damage by Transmission Electron Microscopy*. 2001, Institute of Physics Publishing: **Bristol and Philadelphia**.
19. Packan, N.H. and K. Farrell, *Simulation of first wall damage: Effects of the method of gas implantation*. Journal of Nuclear Materials, 1979. **85-86**: p. 677-681.
20. Zinkle, S. and L. Snead, *Opportunities and limitations for ion beams in radiation effects studies: bridging critical gaps between charged particle and neutron irradiations*. Scripta Materialia, 2018. **143**: p. 154-160.
21. Choyke, W.J., et al., *Helium effects in ion-bombarded 304 stainless steel*. Journal of Nuclear Materials, 1979. **85-86**: p. 647-651.
22. McGruer, J.N., et al., *The effects of sequential and simultaneous helium implantation on void formation in a 304 stainless steel*. Journal of Nuclear Materials, 1978. **74**(1): p. 174-177.
23. Farrell, K., *Experimental effects of helium on cavity formation during irradiation—a review*. Radiation Effects, 1980. **53**(3-4): p. 175-194.
24. Farrell, K. and N.H. Packan, *A helium-induced shift in the temperature dependence of swelling*. Journal of Nuclear Materials, 1979. **85-86**: p. 683-687.
25. Monterrosa, A.M., Z. Jiao, and G.S. Was, *The influence of helium on cavity evolution in ion-irradiated T91*. Journal of Nuclear Materials, 2018. **509**: p. 707-721.
26. Monterrosa, A.M., et al., *The influence of carbon on cavity evolution in ion-irradiated ferritic-martensitic steels*. Journal of Nuclear Materials, 2018. **509**: p. 722-735.
27. Odette, G.R., P.J. Maziasz, and J.A. Spitznagel, *Fission-fusion correlations for swelling and microstructure in stainless steels: Effect of the helium to displacement per atom ratio*. Journal of Nuclear Materials, 1981. **104**: p. 1289-1303.
28. Katoh, Y., et al., *The influence of He/dpa ratio and displacement rate on microstructural evolution: a comparison of theory and experiment*. Journal of Nuclear Materials, 1994. **210**(3): p. 290-302.

29. Sekimura, N., et al., *The effect of helium on the microstructural evolution in PCA as studied by dual beam irradiation*. Journal of Nuclear Materials, 1984. **122**(1): p. 322-326.
30. Katoh, Y., Y. Kohno, and A. Kohyama, *Dual-ion irradiation effects on microstructure of austenitic alloys*. Journal of Nuclear Materials, 1993. **205**: p. 354-360.
31. Suzuki, K., et al., *Cavity growth in dual-ion and electron irradiated HT-9 ferritic stainless steels*. Journal of Nuclear Materials, 1985. **133-134**: p. 632-635.
32. Asano, K., et al., *Microstructural evolution of HT9 under dual-beam charged particle irradiation*. Journal of Nuclear Materials, 1988. **155-157**: p. 912-915.
33. Stoller, R.E., *The influence of helium on microstructural evolution: Implications for DT fusion reactors*. Journal of Nuclear Materials, 1990. **174**(2): p. 289-310.
34. Mansur, L.K., et al., *Control of helium effects in irradiated materials based on theory and experiment*. Journal of Nuclear Materials, 1986. **141-143**: p. 633-646.